Interfacial Superconductivity in FeSe Ultrathin Films on $SrTiO_3$ Probed by *In Situ* Independently Driven Four-Point-Probe Measurements

Asger K. Pedersen,[1,†] Satoru Ichinokura,[1,*] Tomoaki Tanaka,[1] Ryota Shimizu,[2] Taro Hitosugi,[2] and Toru Hirahara[1]
[1]*Department of Physics, Tokyo Institute of Technology, Tokyo 152-8551, Japan*
[2]*Department of Applied Chemistry, Tokyo Institute of Technology, Tokyo 152-8550, Japan*

(Received 17 January 2020; accepted 18 May 2020; published 3 June 2020)

We investigated the superconducting transport properties of the one-unit-cell FeSe ultrathin films epitaxially grown on undoped $SrTiO_3(001)$ (STO) with a well-defined surface structure by *in situ* independently-driven four-point-probe measurements. Our results unambiguously revealed the detection of the two-dimensional electrical conduction of the films without parallel conduction through the underlying substrate, both in the normal and superconducting states. The monolayer film exhibited a superconducting transition at an onset temperature of 40 K. Surprisingly, the onset of superconductivity was constantly observed at 40 K even for three- and five-unit-cell-thick FeSe films, even though the normal resistivity decreased with increasing thickness. These results agree with the picture of the interfacial superconductivity, where only the FeSe/STO interface and/or the adjacent first layer of FeSe becomes superconducting while the upper layers stay in the normal metallic state. The observed T_c is much lower than that reported by a previous *in situ* transport measurement for FeSe/Nb:STO but consistent with the results obtained by *ex situ* measurements for FeSe–undoped STO with a capping layer. This suggests that the capping layer is not an essential factor to limit T_c. We rather propose that the charge transfer from the doped substrate has a key role to achieve the higher temperature superconductivity in the one-unit-cell FeSe.

DOI: 10.1103/PhysRevLett.124.227002

Fourteen years have passed since the discovery of iron-based superconductors [1]. Among them, FeSe has the simplest crystal structure. The highest T_c under normal pressure for a bulk samples is as high as ~8 K [2], but T_c rises sharply with various methods [3,4]. T_c in a FeSe thin film with mono-unit-cell (1-UC) thickness is dramatically increased, reaching a value much higher than 40 K when it is grown on a $SrTiO_3(001)$ (STO) single crystal by molecular beam epitaxy (MBE). Even though intensive studies from various aspects agree that the interface between FeSe and STO plays an essential role in the enhancement of T_c [5–7], there is no satisfactory consensus concerning the microscopic origin because of the scattering of the reported values of T_c. In the MBE-grown 1-UC FeSe/Nb:STO, spectroscopic studies evidenced that the superconducting gap survives up to ~65 K by angle-resolved photoemission spectroscopy (ARPES) [8–10] and scanning tunnel spectroscopy (STS) [11]. On the other hand, *in situ* electrical transport measurements by direct four-point-probe (4PP) detected the resistance drop at the highest $T_c \sim 109$ K [12]. This is outstanding because it has never been reproduced in 1-UC FeSe/STO with a capping layer by the *ex situ* electrical transport measurements, which reported the onset of superconductivity $T_c^{\mathrm{onset}} \sim 40$ K [13]. A similar magnitude of T_c was observed in the electrochemically etched FeSe thin film–STO down to the atomic scale [14]. Furthermore, there is also a debate concerning the localization depth of the superconductivity with respect to the thickness of the film. In Ref. [14], it was shown that T_c^{onset} was constant from $t = 0.6$ to 3 nm and decreased above 3 nm. This conflicts with spectroscopic studies, where the nonsuperconductive nature of 2-UC-thick films is suggested [11].

One can assume that the contradictions explained above are caused by the difference of detailed atomic structure around the interface or the probing depth of the experimental tools [6,7]. The former point was studied in Refs. [15,16], where the local superconducting gap size of FeSe probed by STS was shown to be different with respect to the underlying reconstructed structure of the STO surface. In this Letter, we intended to investigate the latter idea. We prepared 1–5 layers of FeSe on an insulating STO substrate by MBE and performed resistance measurements by the *in situ* direct 4PP method, cooling down the sample to 3 K. This method is not surface sensitive as ARPES or STS and, moreover, the depth of the current path can be systematically controlled by changing the probe spacing [17], enabling the elucidation of the conductivity dimension of the sample. First, we obtained definite evidence that we were measuring the two-dimensional electrical conduction of the films without influence from the underlying STO substrate. Second, we observed a resistance drop with an onset temperature $T_c^{\mathrm{onset}} \sim 40$ K and the film resistance eventually dropped to zero at ~10 K. These features are

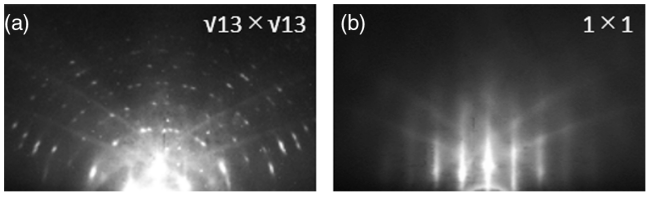

FIG. 1. (a) RHEED pattern of the ultraclean $SrTiO_3$ surface with $\sqrt{13} \times \sqrt{13}$ superstructure spots. (b) RHEED pattern of 1-UC FeSe film after growth.

characteristics of low-dimensional superconductivity. Surprisingly, the above features were observed also for 3- and 5-UC-thick films. This unambiguously suggests that the high-temperature superconductivity essentially locates at the interface of FeSe/STO or the monolayer FeSe without spreading to the upper layers. By combining with previous results, we conclude that the doping level of the STO substrate, either from Nb (conducting bulk) or from oxygen vacancies formed by annealing (conducting surface), is an important factor to obtain high T_c.

Undoped STO substrates ($2 \times 13 \times 0.5$ mm^3) (Shinkosha) substrates were used in this study. For the dc resistive heating, 150-nm-thick Pt films were deposited at the back of the samples [18]. They were degassed at 500 °C in an ultrahigh-vacuum chamber overnight, followed by etching under Se flux at 950 °C for 30 min [11]. Further annealing without flux at 700 °C for 30 min completes the formation of the atomically ultraclean surface of STO evidenced by the sharp $\sqrt{13} \times \sqrt{13}$ periodic patterns in the reflection high-energy electron diffraction (RHEED) [19,20], as shown in Fig. 1(a). After this procedure, the FeSe films were grown *in situ* by coevaporating Fe (99.5%) and Se (99.999%) with a flux ratio of ~1:9 at a substrate temperature of 450 °C, followed by postannealing at 500 °C for 5 min in order to create high-quality films. The growth rate was monitored by observing the RHEED oscillation. Figure S1(a) of the Supplemental Material [21] shows the RHEED oscillation curve of the specular spot during the deposition of "1-UC" sample. One can notice the peak and dip structures very clearly, and the dip indicated by the red dashed line corresponds to the formation of the uniform 1-UC FeSe as judged by our previous STM measurements [15]. Since the beam size of the RHEED (~1 mm) is smaller than the sample size, we deposited 1.3 UC of FeSe in total so that we could be sure that the entire surface was covered with FeSe, and regard it as the 1-UC sample. The RHEED pattern grown in this way is depicted in Fig. 1(b) [and Fig. S1(b)] and it shows 1×1 streaks. We confirmed that the clear streak and oscillation in the RHEED pattern means the formation of high-quality FeSe film by comparing with our own STM studies, as shown in Figs. S1(c)–S1(f) in the Supplemental Material [21]. Subsequently, we transferred this 1-UC FeSe/STO to the measurement room shown in Fig. S2(a), without exposing it to the atmosphere. Thickness dependence of the transport properties was investigated by a cycle of temperature-dependent resistance measurements and further deposition of FeSe on the same specimen.

The 4PP system is a customized model of USM-1400 (Unisoku Co., Ltd.) with a cooling capability from room temperature (RT) down to 3 K. To eliminate the effect of the thermal drift on the resistivity measurements, we used probes with flexible gold wires on the apex to realize soft and stable contact on the surface. The 4PP can be driven independently in the x, y, and z directions by piezoactuators and their movement is observed with a CCD camera. The smallest probe spacing in this measurement was 72 μm as discussed later. In the present Letter, they are aligned in a straight line, as schematically drawn in Fig. S2(b) [21], and used as either current (I^+, I^-) ($|I^+| = |I^-| = I$) or voltage probes (V^+, V^-). The dc current-voltage ($I - V$) characteristic was obtained continuously as a function of temperature. Although the "resistance" $R_{ex} = (V^+ - V^-)/I$ can be extracted from the $I - V$ characteristics by the linear fitting, R_{ex} does not directly correspond to the actual physical quantity. It should be converted to the resistivity ρ by a proper formula depending on the dimensionality of the conducting channel. The state-of-the-art 4PP provides a scheme to probe the dimensionality directly. Figure 2(a) depicts the setup of the measurement. The tips were aligned in the sequence of (1, 2, 4, 3) and used as (I^+, V^+, I^-, V^-). The positions of tips 1, 2, and 4 were fixed and the position of tip 3 was gradually moved closer to tip 4, as indicated by the black arrow. R_{ex} was measured as the probe spacing between probes 3 and 4 was changed.

The theoretical formula of R_{ex} depends on the dimensionality of the current path. In two- and three-dimensional cases, it is expressed as

$$R_{ex} = \frac{\rho_{2D}}{2\pi}\left(\ln\frac{1}{|s_{12}|} + \ln\frac{1}{|s_{34}|} - \ln\frac{1}{|s_{24}|} - \ln\frac{1}{|s_{13}|}\right), \quad (1)$$

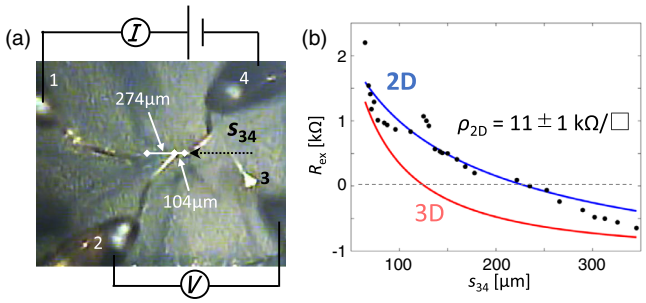

FIG. 2. 4PP measurements on the FeSe/$SrTiO_3$. (a) Photograph of the setup for the dimensionality probing with the schematic circuits. Probe 3 is moved in the horizontal direction, whereas probes 1,2, and 4 are fixed. (b) $R_{ex} = V/I$ in the setup of (a) plotted as a function of the distance between probes 3 and 4. The blue and red lines represent the best results of numerical fitting to Eqs. (1) and (2), respectively.

and

$$R_{\mathrm{ex}} = \frac{\rho_{3\mathrm{D}}}{2\pi}\left(\frac{1}{|s_{12}|} + \frac{1}{|s_{34}|} - \frac{1}{|s_{24}|} - \frac{1}{|s_{13}|}\right), \qquad (2)$$

respectively [22]. Here $\rho_{2(3)\mathrm{D}}$ is 2D (3D) resistivity and s_{ij} is the spacing between the ith and jth probe, estimated from the CCD camera image. The sequence of images during these probe-spacing-dependent measurements are shown in Fig. S3 [21]. In the present set up, s_{12} and s_{24} are fixed at 274 and 104 μm, respectively, and $s_{13} = (378 + s_{34})$ μm, so R_{ex} can be regarded as a function of s_{34} with $\rho_{2(3)\mathrm{D}}$ as the fitting parameter. Both of the above equations expect the sign reversal of R_{ex}. (Note that the sign of R_{ex} can be negative because it is determined by the potential difference of V^+ and V^-.) In the linear arrangement, $R_{\mathrm{ex}} = 0$ is expected at $s_{34} = 231$ μm for Eq. (1) and 126 μm for Eq. (2), respectively. The experimental data of $R_{\mathrm{ex}}(s_{34})$ in the 1-UC FeSe/STO obtained at 250 K are plotted in Fig. 2(b). The R_{ex} decreased monotonically and changed its sign at $s_{34} \sim 240$ μm. It is quite close to the expected value for the 2D case, suggesting the two-dimensional conductivity in the 1-UC FeSe/STO. For further confirmation, we compared the numerical fitting of Eqs. (1) and (2) to the dataset. Apparently, Eq. (1) (blue line) shows better agreement to the data than Eq. (2) (red line). From this fitting, $\rho_{2\mathrm{D}} = 11 \pm 1$ kΩ/□ was obtained. This result indicates that the current path is limited in the vicinity of the surface within the thickness as thin as the probe spacing (∼100 μm). Thus, we successfully suppressed the conduction through the substrate by employing an undoped STO. This point will be mentioned again later to discuss the superconducting properties of FeSe.

Once we determine the dimensionality, we can evaluate the two-dimensional resistivity $\rho_{2\mathrm{D}}$ exactly by the following equation, regardless of probe spacing, called the dual configuration method [23–26]:

$$\exp\left(-\frac{2\pi R^A_{\mathrm{ex}}}{\rho_{2\mathrm{D}}}\right) + \exp\left(-\frac{2\pi R^B_{\mathrm{ex}}}{\rho_{2\mathrm{D}}}\right) = 1, \qquad (3)$$

where $R^A{}_{\mathrm{ex}}$ and $R^B{}_{\mathrm{ex}}$ are obtained from $I - V$ characteristics within $I = \pm 300$ μA in configurations A and B: tips (1–4) are used as (I^+, V^+, V^-, I^-) and (I^+, I^-, V^+, V^-), respectively [schematically shown in the inset of Fig. 3(a)]. This method corrects the error of $\rho_{2\mathrm{D}}$ due to the uncertainty of probe spacing caused by thermal drifting during the following temperature-variable measurements.

Figure 3(a) displays $\rho_{2\mathrm{D}}$ of 1–5-UC-thick FeSe films on the STO substrate as a function of temperature T. The distances between probes are ∼100 μm in this measurement. For all the temperature ranges, continuous $\rho_{2\mathrm{D}} - T$ curves were obtained as a result of the soft contact and the dual configuration method. Upon cooling from RT, the $\rho_{2\mathrm{D}}$ basically shows a metallic behavior except for the peak

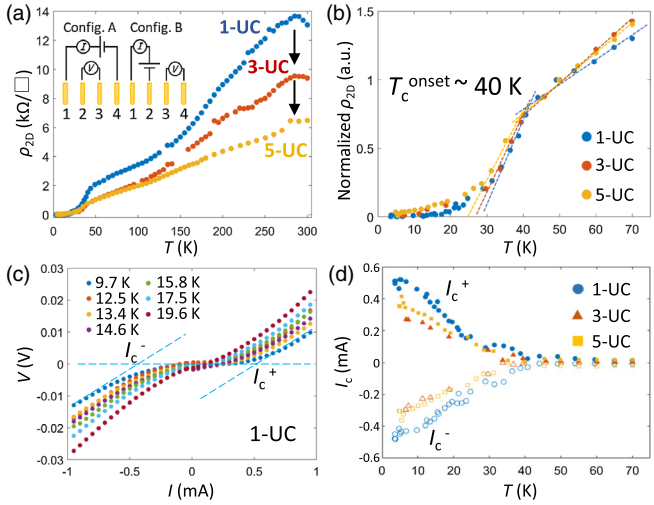

FIG. 3. Results of the temperature-dependent transport measurements on the FeSe/$SrTiO_3$. (a) Zero-bias two-dimensional resistivity $\rho_{2\mathrm{D}}$ in 1-, 3-, and 5-UC FeSe plotted in the full temperature range. The black arrows indicate the change of the normal-state resistivity by the deposition. (Inset) Shows circuits for the dual configuration measurements. (b) $\rho_{2\mathrm{D}}$ normalized by the value at 50 K, plotted around the onset of the superconductivity. T_c^{onset} is defined as the crossing point of linear fitting above and below the transition. (c) $I - V$ characteristics at fixed temperatures from 10 to 20 K. For each curve, the critical current $I_c^{\pm}$ is defined at the point where the straight line extracted from nonsuperconducting sides crosses the abscissa. (d) $I_c^{\pm}$ plotted as a function of the temperature.

structure at 280 K, which likely originates from the freezing of the subtle residual carriers of the STO substrate. Importantly, the films show a sudden drop in $\rho_{2\mathrm{D}}$ around $T_c^{\mathrm{onset}} \sim 40$ K. In the 1-UC FeSe, $\rho_{2\mathrm{D}}$ dropped from 2 kΩ at 40 K to zero at ∼13 K. This strongly reveals the occurrence of superconductivity at an elevated temperature than $T_c \sim 8$ K in the bulk. Note that we observed a tremendous change of resistivity in the order of kΩ within the temperature range of 30 K, which is much larger than that shown in Ref. [12]. This again unambiguously indicates that we detected the essential conductivity of the FeSe film by employing the undoped-STO substrate. Such slow resistance drop is also a characteristic of low-dimensional superconductivity influenced by fluctuation [13,23–27]. One also finds the absence of thickness dependence of onset temperature of the superconductivity even though the normal-state resistivity decreased by increasing the film thickness. This is more prominently observed when we normalize the measured $\rho_{2\mathrm{D}}$ with that at 50 K. The normalized $\rho_{2\mathrm{D}}$ in the vicinity of the transition is shown in Fig. 3(b). The onset temperature T_c^{onset}, defined as the crossing point of linear fitting above and below T_c^{onset}, stayed at 40 K regardless of the thickness. This is consistent with *ex situ* thickness-dependent transport studies with electrochemically etched FeSe thin film–STO, where T_c^{onset}

TABLE I. Summary of the superconducting transition temperature in the FeSe ultrathin films on the $SrTiO_3$ substrate classified by different experimental methods and film thickness t. Δ means superconducting gap size defined as peak-to-peak energy separation of quasiparticle peaks in the spectrum. Δ is converted to T_c by the relation $2\Delta/k_BT_c \sim 5.5$ (k_B is the Boltzmann constant) assuming it is the same for the bulk and the film. T_c^{onset} in transport measurement is defined as a crossing point of linear fitting above and below T_c^{onset}. T_c^{onset} in magnetization measurements is defined as the temperature where the diamagnetic response starts.

	Method	Substrate	$\Delta(T_c)$ or T_c^{onset} in 1 UC (K)	T_c^{onset} in $t \geqq 2$ UC (K)	Ref.
In situ	ARPES	Nb doped	13–15 meV (~55–65)	No SC	[8–10]
	STS	Nb doped	20 meV (~84)	No SC	[11]
		Insulating	15 meV (~65)	…	[29]
	Transport	Nb doped	109	…	[12]
		Insulating	40	40	This Letter
Ex situ	Transport	Insulating	40	40–53	[11,13,14]
	Magnetization	Nb doped	65–85	…	[30,31]
		Insulating	21–25	…	[13]

is constant at ~40 K for films with thicknesses of 0.6–3 nm [14].

Below the onset temperature of superconductivity, $I-V$ curves become nonlinear for large I. The evolution of nonlinearity at 10–20 K for the one monolayer sample in configuration A is shown in Fig. 3(c). The plateau near zero bias corresponds to the zero resistivity and it becomes finite by increasing the current. Note that $I-V$ characteristics obtained by point probes do not show a jump from zero voltage to Ohmic behavior typical for a superconductor. Since the current spreads radially from the drain I^+ probe in the present setup, the current density is not uniform and decreases as the distance from the drain probe becomes larger. Thus, the broken superconductivity is gradually recovered when the voltage probe is placed far from the drain probe, and this results in the blunt transition we have observed in our $I-V$ curves. For temperatures higher than 13 K, a finite slope is observed even near zero bias due to fluctuation effects of low-dimensional superconductivity, as discussed above.

Even though the $I-V$ curves shown in Fig. 3(c) are complicated, we can still distinguish the nonlinear one from the linear one and extract the "critical current" $I_c^{\pm}$, where the superconductivity breaks due to the large current. It is defined at the point where a straight line extracted from the nonsuperconducting sides crosses the abscissa. I_c^{+} and I_c^{-} symmetrically approached each other as the sample was warmed up, as plotted in Fig. 3(d). Finally, they collapsed into zero at 40 K, which is in good agreement with the T_c^{onset} in the $\rho_{2D}-T$ curves. The 3 and 5 UC showed the same closing temperature as the 1 UC, supporting the thickness-independent nature of superconductivity in FeSe ultrathin film on STO [28].

In the following two paragraphs, we discuss the interfacial superconductivity and origin of the enhancement of T_c in FeSe/STO, by comparing the present Letter with the literature. Table I summarizes the T_c or the superconducting gap size Δ in ultrathin FeSe films grown on STO found in this Letter and those reported previously. Δ can be converted to T_c by the relation $2\Delta/k_BT_c \sim 5.5$ (k_B is the Boltzmann constant), assuming that it is the same as that of bulk FeSe. Based on this table, first, let us discuss the spatial distribution of the superconductivity in this system. For FeSe films thicker than 2 UC, nonsuperconducting behavior was observed by ARPES [9] and STS [11], while $T_c \sim 40$ K has been reproducibly seen in *ex situ* transport measurements [11,13,14]. Many studies point out that the first UC or the interface of FeSe/STO dominantly becomes superconducting at high temperatures, while the upper layers may remain metallic [5–7]. The interfacial superconductivity cannot be detected by ARPES and STS when two or more unit cells exist because of the surface sensitivity. On the other hand, transport measurements can detect the interfacial superconductivity even in the thicker films since the current can reach the interface through the upper normal-metallic region. The present results in Fig. 3(a) support this interpretation; as indicated by black arrows, the normal-state resistivity at high temperature decreases as the film becomes thicker. However, T_c^{onset} is not affected and the superconducting properties are thickness independent.

Next, we focus on the T_c for the 1 UC. We observed $T_c^{\mathrm{onset}} \sim 40$ K with the present *in situ* transport measurements and this is in good agreement with the reports performed *ex situ* with capping layers [11,13,14] rather than one done *in situ* which showed a T_c of 109 K [12]. Up to now, the capping layer has been thought to decrease T_c from the value of pristine FeSe thin films [7]. The present results do not agree with the suggestion. Rather, we propose that the difference of the observed T_c can be explained by the difference in electron doping from the STO substrate to the interface as follows. According to Table I, FeSe grown on the Nb-doped STO always has a higher T_c than that grown on the insulating substrate irrespective of the measurement method. This implies that carriers in the substrate should contribute to electron doping to the interface and the enhancement of T_c. Actually, T_c higher than 65 K has been observed only

in the FeSe/Nb:STO. Some authors claim that the conductivity of the substrate is not necessary to induce high-temperature superconductivity to FeSe because two-dimensional electron gas (2DEG) is formed on the surface of STO during the annealing procedure of the substrate treatment [29]. However, the formation of 2DEG strongly depends on the treatment temperature [32]. This should originate from the density of oxygen vacancies at the surface, which can be estimated from the reconstruction structure. Our FeSe was grown on STO with the $\sqrt{13} \times \sqrt{13}$ reconstructed surface, which is known to contain fewer oxygen vacancies compared to others [18]. The conductivity through STO was investigated by Leis *et al.* at different stages of thermal reduction by means of a similar 4PP technique [33]. According to their study, annealing at 600 and 900 °C is enough to form the 2D and 3D conducting channel in STO, respectively. As discussed above, however, the conductivity is suppressed through the bulk STO in the present study, even though we used 900 °C to obtain the ultraclean surface. The contradiction between those results is explained by the difference for heating treatment; ac current was used in Ref. [33], while dc was used in the present Letter. The oxygen vacancies accumulate near the electrical contact at the edge of the sample, far from the probing area by 4PP, due to the electrical migration by the dc current [18]. We also confirmed the insulating nature of the STO surface before the growth of FeSe by two-terminal measurements, where a resistance of 11 MΩ was detected (see Fig. S4 in the Supplemental Material [21]). Therefore, in the present substrate, both bulk and surface of STO have poor conductivity and a very small amount of carriers. Thus, we conclude that whether the bulk and surface of STO is conducting or not has a significant effect on the T_c enhancement of the interfacial superconductivity of FeSe/STO.

In summary, we investigated the superconductivity of the 1–5-UC-thick FeSe ultrathin films on STO by *in situ* 4PP transport measurements. We observed a clear two-dimensional conductivity and superconducting transition with the onset at 40 K. The superconducting features were the same even for the 3- and 5-UC-thick films and strongly indicated the interfacial nature of the superconductivity. Our results clarify the long-standing puzzle of a relatively low T_c around 40 K in all transport experiments. We propose that the smaller amount of charge transfer from the insulating substrate to the FeSe/STO interface compared to the works performed on conductive STO substrates is the origin of the lower T_c. This reconfirms the importance of the charge accumulation from the substrate to the interface.

We thank R. Hobara at the University of Tokyo for the fruitful discussion. This work has been supported by Grants-In-Aid from Japan Society for the Promotion of Science (Grants No. 15H05453, No. 18H03876, No. 18H03877, No. 19K15443), the Murata Science Foundation, the Asahi Glass Foundation, and the Sumitomo Foundation. Ohsumi Yoshinori Research Support for Basic Science (Tokyo Institute of Technology). A. K. P. and S. I. contributed equally to this work.

*Corresponding author.
ichinokura@phys.titech.ac.jp
†Present address: Department of Physics, Technical University of Denmark, Lyngby, 2800 Kgs, Denmark.

[1] Y. Kamihara, H. Hiramatsu, M. Hirano, R. Kawamura, H. Yanagi, T. Kamiya, and H. Hosono, J. Am. Chem. Soc. **128**, 10012 (2006).
[2] F.-C. Hsu *et al.*, Proc. Natl. Acad. Sci. U.S.A. **105**, 14262 (2008).
[3] S. Medvedev *et al.*, Nat. Mater. **8**, 630 (2009).
[4] H. K. Vivanco and E. E. Rodriguez, J. Solid State Chem. **242**, 3 (2016).
[5] L. Wang, X. Ma, and Q.-K. Xue, Supercond. Sci. Technol. **29**, 123001 (2016).
[6] D. Huang and J. E. Hoffman, Annu. Rev. Condens. Matter Phys. **8**, 311 (2017).
[7] Z. Wang, C. Liu, Y. Liu, and J. Wang, J. Phys. Condens. Matter **29**, 153001 (2017).
[8] S. He *et al.*, Nat. Mater. **12**, 605 (2013).
[9] S. Tan *et al.*, Nat. Mater. **12**, 634 (2013).
[10] J. J. Lee *et al.*, Nature (London) **515**, 245 (2014).
[11] W. Qing-Yan *et al.*, Chin. Phys. Lett. **29**, 037402 (2012).
[12] J. F. Ge, Z. L. Liu, C. Liu, C. L. Gao, D. Qian, Q. K. Xue, Y. Liu, and J. F. Jia, Nat. Mater. **14**, 285 (2015).
[13] W.-H. Zhang *et al.*, Chin. Phys. Lett. **31**, 017401 (2014).
[14] J. Shiogai, Y. Ito, T. Mitsuhashi, T. Nojima, and A. Tsukazaki, Nat. Phys. **12**, 42 (2016).
[15] T. Tanaka, K. Akiyama, R. Yoshino, and T. Hirahara, Phys. Rev. B **98**, 121410(R) (2018).
[16] T. Tanaka, K. Akiyama, S. Ichinokura, R. Shimizu, T. Hitosugi, and T. Hirahara, Phys. Rev. B **101**, 205421 (2020).
[17] S. Hasegawa, I. Shiraki, F. Tanabe, and R. Hobara, Curr. Appl. Phys. **2**, 465 (2002).
[18] R. Shimizu, K. Iwaya, T. Ohsawa, S. Shiraki, T. Hasegawa, T. Hashizume, and T. Hitosugi, Appl. Phys. Lett. **100**, 263106 (2012).
[19] T. Ohsawa, R. Shimizu, K. Iwaya, S. Shiraki, and T. Hitosugi, Appl. Phys. Lett. **108**, 161603 (2016).
[20] R. Shimizu, K. Iwaya, T. Ohsawa, S. Shiraki, T. Hasegawa, T. Hashizume, and T. Hitosugi, ACS Nano **5**, 7967 (2011).
[21] See Supplemental Material at http://link.aps.org/supplemental/10.1103/PhysRevLett.124.227002 for information about the experimental details. Figure S1 shows the sample evaluation using reflection high-energy electron diffraction and scanning tunnel microscopy. Figures S2 and S3 show the photographs of the independently-driven four-point-probe instrument. Figure S4 shows the result of two-terminal measurements on the bare $SrTiO_3$ and $FeSe/SrTiO_3$ film.
[22] S. B. Kjeldby, O. M. Evenstad, S. P. Cooil, and J. W. Wells, J. Phys. Condens. Matter **29**, 394008 (2017).

[23] M. Yamada, T. Hirahara, R. Hobara, S. Hasegawa, H. Mizuno, Y. Miyatake, and T. Nagamura, Surf. Sci. Nanotechnol. **10**, 400 (2012).
[24] M. Yamada, T. Hirahara, and S. Hasegawa, Phys. Rev. Lett. **110**, 237001 (2013).
[25] S. Ichinokura, K. Sugawara, A. Takayama, T. Takahashi, and S. Hasegawa, ACS Nano **10**, 2761 (2016).
[26] A. V. Matetskiy, S. Ichinokura, L. V. Bondarenko, A. Y. Tupchaya, D. V. Gruznev, A. V. Zotov, A. A. Saranin, R. Hobara, A. Takayama, and S. Hasegawa, Phys. Rev. Lett. **115**, 147003 (2015).
[27] R. Schneider, A. G. Zaitsev, D. Fuchs, and H. von Lohneysen, J. Phys. Condens. Matter **26**, 455701 (2014).
[28] We comment on the magnitude of critical current (0.5 mA at 3 K). If we use the simplest approximation that the current only flows through the 1-UC FeSe layer and superconductivity is broken at the position of the voltage electrode, the critical current density (Jc) is estimated as 1.4×10^5 A/cm^2. This is smaller than Jc in Refs. [12,13] by 1 or 2 orders of magnitude, respectively. Since this difference cannot be explained by the T_c, it implies that the effective current density in the film is different due to the certain amount of contribution of the STO substrate. Actually, the samples in Refs. [12,13] have much higher conductivity in the normal state compared to the present Letter.
[29] W. Zhang *et al.*, Phys. Rev. B **89**, 060506(R) (2014).
[30] Y. Sun, W. Zhang, Y. Xing, F. Li, Y. Zhao, Z. Xia, L. Wang, X. Ma, Q.-K. Xue, and J. Wang, Sci. Rep. **4**, 6040 (2015).
[31] Z. Zhang, Y.-H. Wang, Q. Song, C. Liu, R. Peng, K. A. Moler, D. Feng, and Y. Wang, Sci. Bull. **60**, 1301 (2015).
[32] R. Di Capua, M. Radovic, G. M. De Luca, I. Maggio-Aprile, F. M. Granozio, N. C. Plumb, Z. Ristic, U. S. di Uccio, R. Vaglio, and M. Salluzzo, Phys. Rev. B **86**, 155425 (2012).
[33] A. Leis, C. Rodenbücher, K. Szot, V. Cherepanov, F. S. Tautz, and B. Voigtländer, Sci. Rep. **9**, 2476 (2019).